ORIGINAL ARTICLE

Magnetic photocatalysts based on graphene oxide: synthesis, characterization, application in advanced oxidation processes and response surface analysis

Sedigheh Abbasi[1] ⓘ

Abstract

The decomposition rate of methyl orange (MO) is studied in aqueous solution of magnetic photocatalysts based on graphene oxide (GO). ZnO photocatalytic nanoparticles are synthesized with controlled amounts on magnetized graphene oxide and two photocatalytic samples including GFZ1 and GFZ2 are prepared for use in advanced oxidation process. The characterization of the synthesized photocatalysts is done by XRD, FTIR and VSM. The crystal structure of magnetic Fe_3O_4 nanoparticles as well as photocatalytic ZnO nanoparticles on the graphene oxide network has been confirmed by XRD analysis in both synthesized samples. FTIR analysis of both GFZ1 and GFZ2 also shows the stretching vibration of Fe–O and Zn–O bonds in Fe_3O_4 and ZnO, respectively. The superparamagnetic properties of both samples can be confirmed using VSM analysis. It is also observed that with the increase of ZnO nanoparticles in GFZ2, the magnetic properties decrease compared to GFZ1. The effect of irradiation time time (between 5 and 40 min), weight fraction of the synthesized photocatalysts (0.1%wt, 0.2%wt, and 0.3%wt) and pH of the suspension (3, 7, and 11) on the changes in MO decomposition rate was investigated and the response surface method (RSM) was used to study the effect of the simultaneous change of two parameters of the mentioned factors on the MO removal efficiency. The results show that with the increase of irradiation time and also the weight fraction of both photocatalysts, the decomposition rate of MO also increases significantly. So that in all time intervals and weight fractions, the photocatalytic activity of GFZ2 is much higher than that of GFZ1. The effect of pH also shows that the maximum and minimum decomposition rates occur in acidic and neutral conditions, respectively.

Keywords Graphene oxide · Superparamagnetic · Photocatalysts · Decomposition rate · Response surface method

Introduction

Carbon materials with two-dimensional (2-D) structure as well as their derivatives have been considered in various research fields due to their special features. One of the most common and widely used derivatives of 2-D carbon structures is graphen oxide (GO) which is specially used in the preparation of composites, catalytic processes, electronic industries and water treatment (Gan 2018; Abbasi et al. 2020; Tao et al. 2023). The significant use of GO in water treatment can be due to the high surface-to volume ratio, specific surface area and hydrophilic functional groups on

its surface. Oxygen-containing functional groups such as hydroxyl and carboxylic acid on the surface of GO increase the tendency of dye organic contaminant to be adsorbed on the surface of GO (Yuan, et al. 2012; Abbasi 2020). Unfortunately, dye pollutants that produced in the effluents of industrial plants enter the environment and cause many problems for living organisms due to their toxicity (Abbasi 2020, 2019). Therefore, the removal of such pollutants is one of the main concern of environmental activists. Extensive studies have been performed on methods for removing dye pollutants including physical, chemical, catalytic and biological methods (Abbasi et al. 2020; Abbasi 2018). Advanced oxidation process (AOP) is one of the techniques that can be applied for elimination of dye organic pollutants with high efficiency (Abbasi 2022a, 2021a). One of the most important advantages of the AOP is the production of non-toxic and environmentally friendly products after decomposition of pollutants (Zhu et al. 2015; Abbasi and

✉ Sedigheh Abbasi
  s.abbasi@esfarayen.ac.ir; abasi_1362@yahoo.com

1 Central Research Laboratory, Esfarayen University
  of Technology, Esfarayen, North Khorasan, Iran

a.M.-S. Ekrami-Kakhki, and M. Tahari 2019). The AOP is based on the use of semiconductor metal oxides with a wide band gap (such as ZnO, SnO$_2$ and TiO$_2$) as photocatalyst. Exposure of photocatalysts to UV radiation provides the possibility for electron excitation and displacement from the capacitance layer to the conduction layer. (Abbasi et al. 2017a; Kim et al. 2015). The electron displacement between capacitance layer and conduction layer leads to the creation of a negatively charged electron (e$^-$) in the conduction layer and a positively charged hole (h$^+$) in the capacitance layer (Abbasi et al. 2017b; Abdel-Messih et al. 2013). The wide band gap of the utilized photocatalysts reduces the stability of the produced e$^-$–h$^+$ pairs, which leads to rapid recombination and reduction of removal efficiency of pollutants (Ghaderi et al. 2015; Abbasi and Hasanpour 2017a). The combination of photocatalysts and GO creates a new structure of photocatalysts that dramatically reduces the problem of rapid recombination of the e$^-$–h$^+$ pairs. Duo to the fact that the reaction of electron and holes with oxygen and water causes the formation of radical species such as hydroxyl (Reddy et al. 2015; Gao and Sun 2014). This radicals play a significant role in the decomposition of organic pollutants. Hence, increasing the stability of produced e$^-$–h$^+$ pairs increases the number of radicals that participate in the redox reaction (Ghaderi et al. 2018; Roozban et al. 2017a; Abbasi et al. 2021). Thereupon, new GO based photocatalytic nanocomposites have the potential to successfully increase the electron–hole pairs stability and the number of oxidizing radicals. Duo to the importance of the electron–hole pairs stability to increase the removal efficiency of pollutants, the main purpose of this study is the synthesis of magnetic nanocomposites based on GO. The main reason for using the magnetic nanoparticles (Fe$_3$O$_4$) in the nanocomposite structure is the ease of removal of photocatalysts from the system after the decomposition process. In the synthesized photocatalytic nanocomposites. In the synthesized photocatalysts, the content of ZnO nanoparticles as photocatalytic nanoparticles is controlled so that two types of nanocomposites contain a constant amount of GO and Fe$_3$O$_4$ and different amounts of ZnO are prepared. Methyl orange (MO) is used as a dye pollutant to investigate the photocatalytic behavior. The results of MO removal efficiency are evaluated using the response surface method (RSM).

Experimental

Materials

The chemicals used in this study include methyl orange (MO, 99%, Merck) as dye contaminant, Zinc chloride (ZnCl$_2$, 99.9%, Merck), graphen oxide (GO, is provided by Novin Nano Negasht Company, Iran), Ethylene glycol (EG,

99.9%, Merck), Ferric acetylacetonate (Fe(acac)$_3$, Merck) as precursor of magnetic nanoparticles and Ammonium acetate (NH$_4$Ac, NH$_4$CH$_3$CO$_2$, Merck). All the mentioned chemicals are analytical grade and are used without any further purification.

Synthesis of magnetic photocatalysts

In order to synthesize the magnetic photocatalysts based on GO, the flowing is done. First, a suspension containing 45 mg of GO and 45 mL of EG is prepared and placed on a magnetic stirrer at 600 rpm for 30 min. Then, 0.225 g of Fe(acac)$_3$ is added to the above suspension as a precursor of magnetic nanoparticles (Fe$_3$O$_4$) and placed in an ultrasonic bath for 30 min for complete mixing. Ionization of Fe(acac)$_3$ in water causes the formation of iron ions (Fe^{+3}). Duo to the positive charge of iron ions, it is possible to adsorb iron ions on the surface of GO. The established gravity can be attributed to the presence of oxygen-containing groups on the GO surface. By binding iron ions, the nucleation process is provided for the formation magnetic nanoparticles of Fe$_3$O$_4$. Then, 1.5 g of ammonium acetate is poured into the mixture and the final suspension is transferred to an autoclave and placed at 200 °C for 24 h. The applied ammonium acetate can be used as reducing agent of Fe^{3+} to Fe$_3$O$_4$. Then, the autoclave is placed in laboratory to bring it to room temperature. Finally, the synthesized magnetic GO (GO-Fe$_3$O$_4$) is filtered, washed and dried at 60 °C for 12 h. The next step, in preparing the magnetic photocatalysts is the synthesis of photocatalytic ZnO nanoparticles on the surface of GO-Fe$_3$O$_4$. For this purpose, 0.1 g of prepared GO-Fe$_3$O$_4$ is dispersed in 40 mL of H$_2$O and mixed using an ultrasonic bath for 30 min. Then, the desired amount of ZnO (0.05 g and 0.1 g) as precursor of ZnO nanoparticles is added to the suspension of GO-Fe$_3$O$_4$. The variation of ZnCl$_2$ amount can leads to the different content of ZnO nanoparticles on the surface of GO-Fe$_3$O$_4$. The ionization of ZnCl$_2$ in water leads to the formation of Zn^{+2}. The produced Zn^{+2} ions can adhere on the surface of GO-Fe$_3$O$_4$ through the functional groups. The temperature of suspension is then raised to 90 °C. While the suspension is placed on a high-speed magnetic stirrer, 5.3 mL of sodium hydroxide solution (NaOH, 5 M) is added drop wise. Addition of NaOH solution causes the formation of amorphous ZnO nanoparticles on the surface of GO-Fe$_3$O$_4$. To convert the of amorphous ZnO nanoparticles to crystalline structure, the prepared powder is transferred to a furnace at 300 °C for about 3 h. The synthesized samples are identified as GFZ1 and GFZ2. The precursor amount of ZnO nanoparticles in the GFZ1 and GFZ2 samples is equal to 0.05 and 0.1, respectively. Synthesized samples are characterized using Fourier transform infrared (FTIR, Tensor 70), X-ray diffraction pattern (XRD, PHILIPS-binary

diffract meter, Bruker D8 Advance) and vibrating sample magnetometer (VSM, Meghnatis Daghigh Kavir Co., Iran).

Photocatalytic experiments

Photocatalytic experiments are based on the removal of MO from water. The variables affecting the removal efficiency of MO which are investigated in this study include irradiation time (with intensity about 13,000 Lumen), photocatalysts concentration and pH of suspensions. For experiments, a photo reactor equipped with a water circulation system is applied to control the temperature, a stirrer to even out the suspension and a UV lamp (150W, $\lambda = 247.3$ nm, UVC). To prepare the contaminant solution, the concentration of MO is selected to fix at 10 ppm. In each series of experiments, 0.1, 0.2 and 0.3%wt of the synthesized photocatalysts are dispersed into the MO solution and the pH of solution is adjusted to 3, 7 and 11. After preparing the suspensions and adjusting the concentration and pH, all suspensions are stirred in a dark room for one hour. Then filter 3 mL of suspensions to separate the photocatalysts and measure the absorption of the MO at 464 nm using a spectrophotometer. The measured absorbance, which is proportional to the MO concentration, is recorded as A_0 or C_0. The prepared suspensions are then transferred into a photoreactor and irradiation begins. At intervals of 5 min, the amount of absorption proportional to the concentration is measured in a manner described above. The amount of measured adsorption and concentration are considered as A_t or C_t, respectively. The decomposition rate of MO can be calculated using Eq. 1 (Ghaderi et al. 2015; Abbasi and Hasanpour 2017b).

$$\text{Decomposition rate}(\%) = \frac{A_0 - A_t}{A_0} \times 100 = \frac{C_0 - C_t}{C_0} \times 100 \quad (1)$$

Statistical studies of the results are performed using response surface methodology (RSM). In this method, the dual influence of effective variables on the fixed level of the third variable is investigated. The Minitab release software (ver 13.1) is used for RSM.

Results and discussion

XRD study

The XRD patterns of the synthesized GFZ1 and GFZ2 are demonstrated in Figs. 1 and 2, respectively. The main characteristic peaks of GO, ZnO and Fe_3O_4 can be confirmed according to the results of these two Figures. The appeared peak around $2\theta = 11°$ in the both Figures belong to the (002) lattice plane of GO. Meanwhile, the characteristic peaks that is centered at $2\theta = 30.25°, 35.61°, 57.35°$ and $63.25°$ confirm the presence of Fe_3O_4 with cubic structure (Abbasi et al. 2020). The generated peaks in the mentioned situations are related to the (220), (311), (511) and (440) Bragg reflection plane of Fe_3O_4. In addition of belonged peaks to the GO and Fe_3O_4 in both Figs. 1 and 2, several peaks can be detected at $31.87°, 34.5°, 36.3°, 47.68°, 56.56°$ and $62.65°$. According to the previous reported results these observed peaks may be related to the (100), (002), (101), (102), (110) and (103) lattice plane of ZnO nanoparticles (Ghaderi et al. 2018; Roozban et al. 2017a). According to the observed peaks, it is possible to confirm the successful synthesis of ZnO nanoparticles in both prepared photocatalytic samples. The comparison between the main peaks of ZnO nanoparticles in GFZ1 and GFZ2 shows that the intensity of all the peaks in the GFZ2 is higher than the GFZ1. The increase in the intensity of the characteristic peaks confirms the enhancement the

Fig. 1 XRD pattern of the synthesized GFZ1
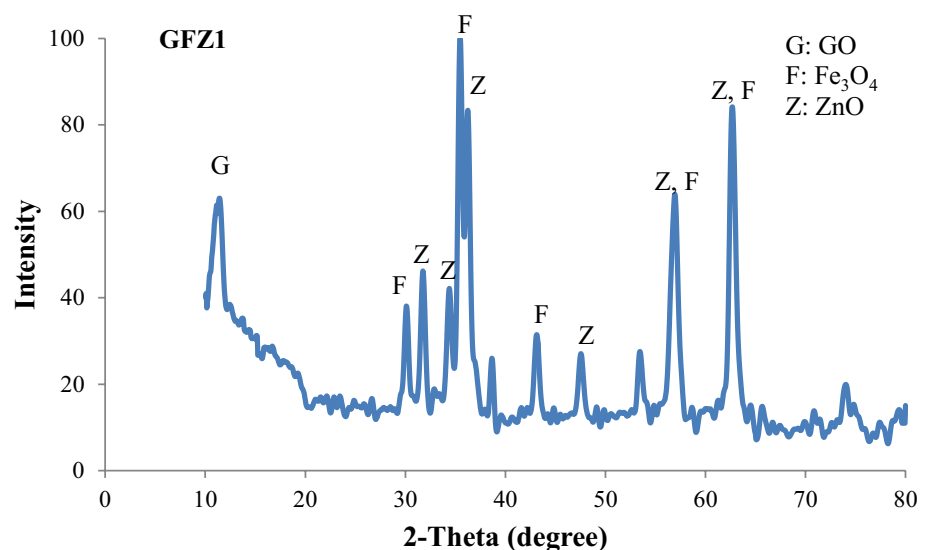
Fig. 2 XRD pattern of the synthesized GFZ2
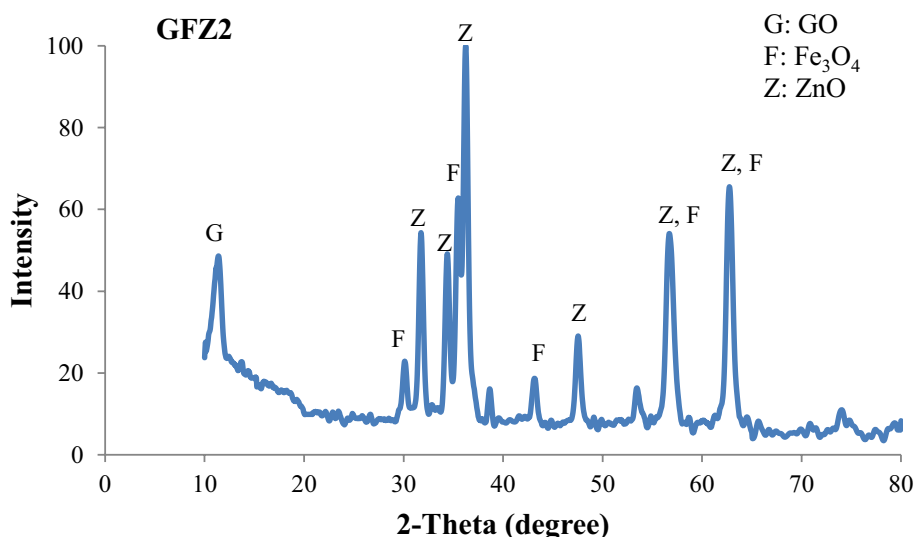
amount of ZnO nanoparticles in GFZ2, which is attributed to the amount of applied ZnCl2 in the synthesis of GFZ2.

FTIR study

FTIR analysis can confirm the structure of prepared photocatalysts. Figures 3 and 4 demonstrate the FTIR spectra of the synthesized GFZ1 and GFZ2, respectively. The analysis of appeared peaks in Fig. 3 justify the bonds between zinc and oxygen (Zn–O) in ZnO which is located at 445 cm^{-1} (Ghaderi et al. 2018; Zak et al. 2011). Stretching vibration of iron and oxygen bonds (Fe–O) that is presented in Fe_3O_4 can be observed at 572 cm^{-1} (Abbasi 2021a; Abareshi et al. 2010). Symmetric and asymmetric stretching of zinc carboxylate appears at 1374 cm^{-1} and 1645 cm^{-1}. The presence

of hydroxyl groups (O–H) in the surface of GFZ1 causes a broad peak at 3430 cm^{-1} (Dastan et al. 2017; Abbasi et al. 2015). Besides the mentioned peaks in Fig. 3, there peaks are located at 1081 cm^{-1}, 1425 cm^{-1} and 1602 cm^{-1} that may be assigned to stretching between carbon and oxygen (C–O) bonds in alkoxy groups, bending vibration of $=CH_2$ and sp^2-hybridized of C=C, respectively (Abbasi 2021a; Zak et al. 2011; Dastan et al. 2016). The analysis of FTIR spectra of GFZ2 that is illustrated in Fig. 4, confirm the formation of ZnO and Fe_3O_4. So that, two pecks at 452 cm^{-1} and 570 cm^{-1} are belonged to Zn–O bonds of ZnO and Fe–O bonds of Fe_3O_4. The intensity of the peak belonging to Zn–O bonds in the GFZ2 is higher than the GFZ1. This indicates an increase in the formation of ZnO in the GFZ2 compared to the GFZ1. As can be seen, the results

Fig. 3 FTIR spectra of the synthesized GFZ1
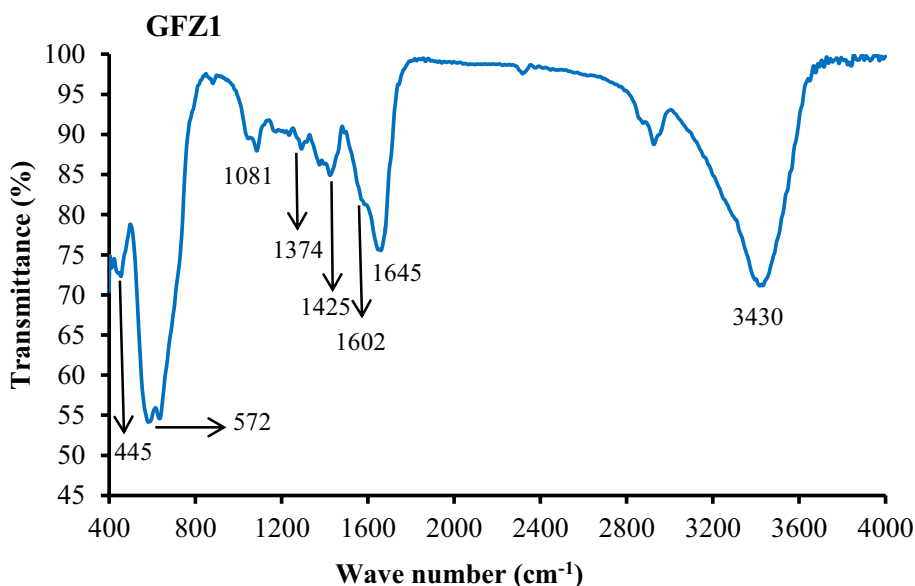
**Fig. 4** FTIR spectra of the synthesized GFZ2

Fig. 5 Magnetization curve for GFZ1
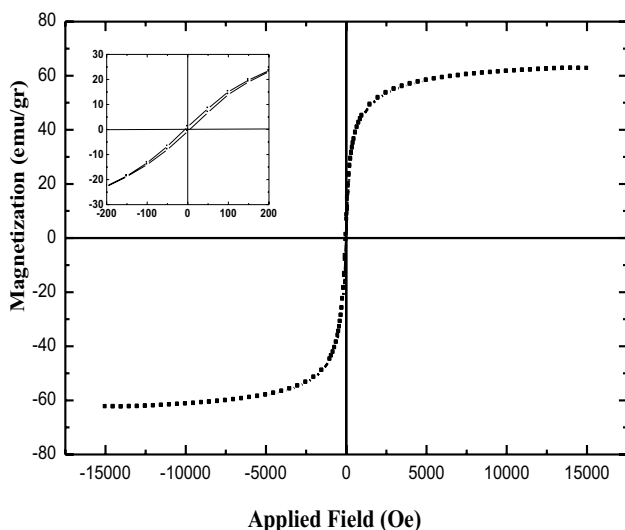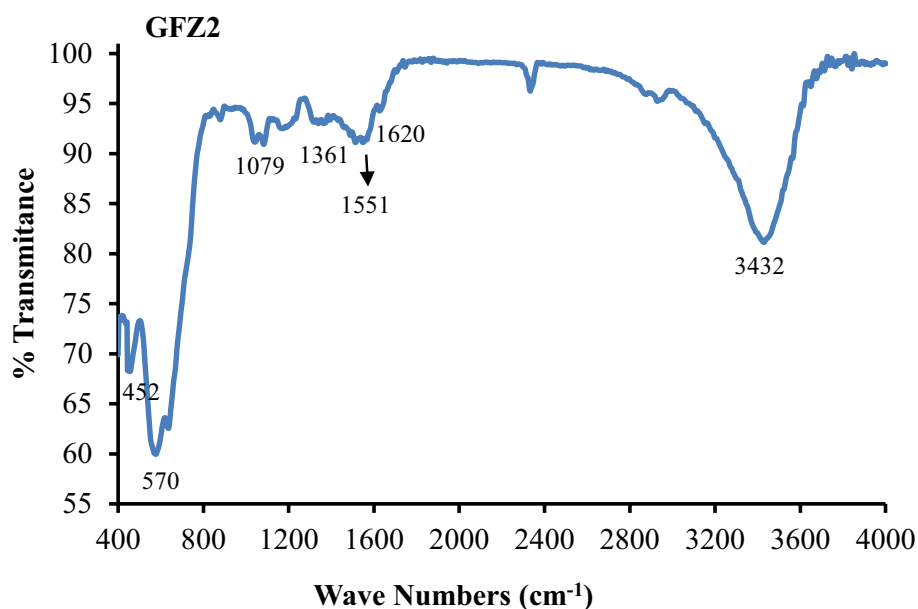
Fig. 6 Magnetization curve for GFZ2

of FTIR is in agreement with XRD results. The presence of GO in GFZ2 can be confirmed by sp^2-hybridization of C=C that is centered at 1620 cm^{-1}. The peak at 1551 cm^{-1} may be belonged to =CH2 groups. Meanwhile, the peaks at 1079 cm^{-1} and 1361 cm^{-1} can be attributed to alkoxy groups and C–OH, respectively.

VSM study

The magnetization behavior of GFZ1 and GFZ2 can be analyzed based on Figs. 5 and 6, respectively. Examining the magnetization curves of both photocatalysts depicts that there is no any hysteresis Loop. Thus, the superparamagnetic
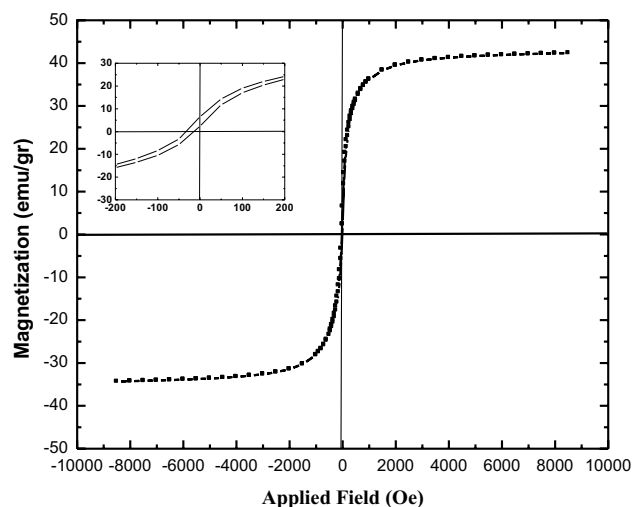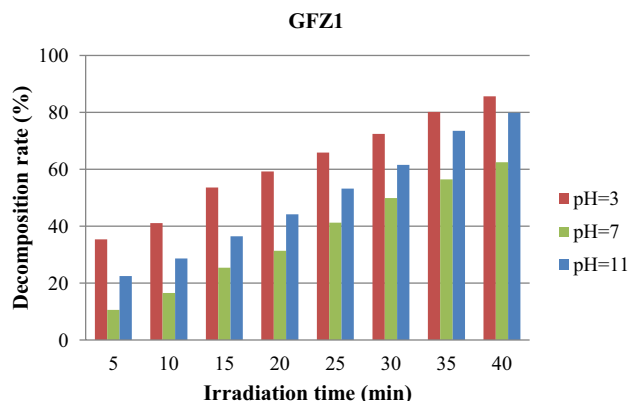
property of GFZ1 and GFZ2 can be confirmed. As can be seen in Figs. 5 and 6, the comparison between the saturation magnetization values of GFZ1 (69.57 emu/g) and GFZ2 (42.35 emu/g) indicates that the saturation magnetization of GFZ1 is higher than that of GFZ2. The decrease in the saturation magnetization of the GFZ2 compared to the GFZ1 may be due to the increase in the photocatalytic ZnO nanoparticles. So that the FTIR and XRD results also confirmed the higher amount of ZnO nanoparticles in the GFZ2 compared to the GFZ1. Examining the value of the coercive field in Figs. 5 and 6 indicates that in both GFZ1 and GFZ2, no significant amount of it is observed and it can be ignored. Also, according to the magnetic curves, it can be seen that the GFZ1 and GFZ2 have a remnant magnetization of 1.123

and 6.57, respectively. According to the values of the magnetic parameters of the GFZ1 and GFZ2, the super paramagnetic property of both samples is proved.

Decomposition rate study

The variation of MO decomposition rate with respect to the irradiation time and pH using GFZ1 and GFZ2 are presented in Figs. 7 and 8, respectively. According to the presented results it is clear that in all pH values, the decomposition rate increases significantly with increasing the irradiation time. The increasing effect of irradiation time on decomposition rate can be attributed to the amount of electron excitation and electron displacement from the capacitance layer to the conduction layer (Navidpour et al. 2019; WANG, X., S. YAO, and X. LI 2009). Therefore, with increasing the electron transfer, the amount of created electron–hole pairs, which is very effective in the production of free radicals and oxidation of pollutants, increases dramatically (Fakhrzad et al. 2019; Roozban et al. 2017b). The results of the pH effect show that the change in the pH of suspension causes the significant variations in the decomposition rate of MO. In acidic suspensions (pH=3), the decomposition rate of the MO is the highest and with increasing the pH to the neutral range (pH=7), the decomposition rate of MO decreases significantly. One of the most effective factors that increases the efficiency of removing pollutants in acidic conditions is the high amount of free hydrogen ions in the reaction medium. Because dissolved oxygen in the suspension containing pollutants and photocatalysts can be absorbed by hydrogen ions and form radical species such as active hydroxyl radicals (Abbasi 2021a). The created radicals have the ability to destroy pollutants. Therefore, with the intensity of acidic conditions and the increase in the amount of free hydrogen ions in the solution, the amount of destructive radicals also increases, and this improves the decomposition of pollutants
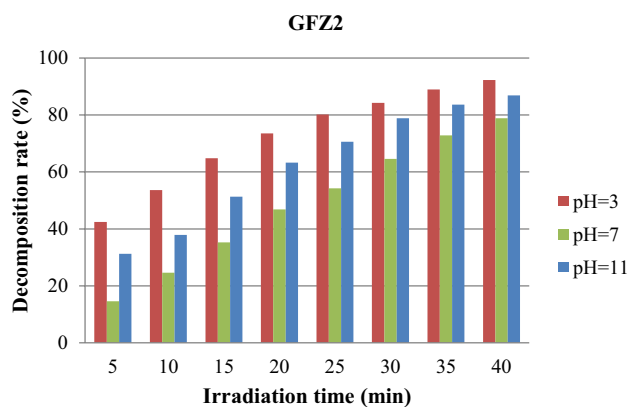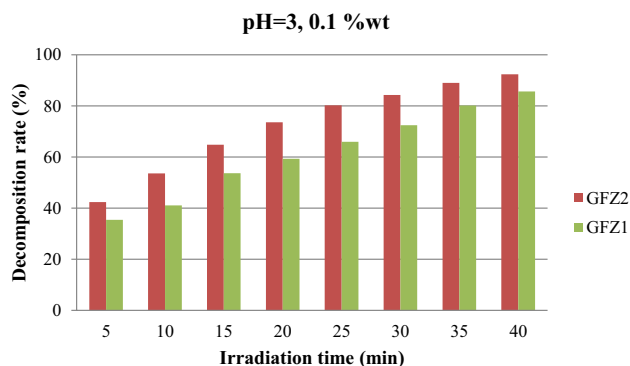
in acidic conditions compared to neutral and alkaline conditions (Abbasi 2021b). The comparison between the changes MO degradation using GFZ1 and GFZ2 with respect to the irradiation time at pH=3 and photocatalyst concentration of 0.1%wt is shown in Fig. 8. As can be seen, in all the time intervals of irradiation, the strength of MO degradation in the presence of the GFZ2 is much higher than the GFZ1. The change in the amount of ZnO nanoparticles in the GFZ1 and GFZ2 is the most important factor in changing the photocatalytic activity of these two samples. In fact, by increasing the amount of photocatalytic ZnO nanoparticles in the sample, the amount of photocatalytic activity as well as the decomposition of MO increases. Therefore, as the XRD, FTIR and VSM results proved, the GFZ2 contains a higher amount of ZnO nanoparticles. Therefore, it is expected that the photocatalytic activity of the GFZ2 is also higher than the GFZ1, and the results presented in Fig. 9 confirm this. Similar results have been obtained to compare the photocatalytic activity of these two samples at other pHs (pH=7

Fig. 8 The variation of MO decomposition rate with respect to the irradiation time and pH using GFZ2

Fig. 7 The variation of MO decomposition rate with respect to the irradiation time and pH using GFZ1

Fig. 9 The comparison between the changes MO degradation using GFZ1 and GFZ2, at pH=3 and 0.1%wt

and pH = 11) and photocatalyst concentrations (0.2%wt and 0.3%wt) (results not presented).

The variation of MO decomposition rate with respect to the irradiation time and weight fraction of GFZ1 and GFZ1 is illustrated in Figs. 10 and 11, respectively. As can be seen, with the increase in the concentration of both photocatalysts from 0.1%wt to 0.3%wt, the decomposition rate also increases. In fact, the increase in photocatalytic activity with increasing photocatalyst concentration is due to several main reasons. Firstly, with the increase in the concentration of the photocatalyst, the active contact surface also increases, which improves the contact of the pollutant with the photocatalyst surface, and a larger amount of the pollutant can bind to the photocatalyst surface in each time period. Secondly, with the increase in the concentration of the photocatalyst, the surface that is exposed to the radiation of the light source also increases, so it is possible to excite a larger number of valence layer electrons and subsequently transfer the excited electrons to the conduction layer. As a result, more electron–hole pairs are produced, which play a fundamental role in photocatalytic activity and subsequent decomposition (Abbasi et al. 2020; Abbasi 2022b). Thirdly, increasing the concentration of the photocatalyst and subsequently increasing the amount of electron–hole pairs causes an increase in the production of oxidizing radical species (Abbasi 2019). The comparison between the changes MO degradation using GFZ1 and GFZ2, at pH = 3 and 0.1%wt is shown in Fig. 12. It can be observed that the decomposition rate of MO using GFZ2 is higher than that of GFZ1. It may be attributed to the ZnO content of these two samples. As it is described before, ZnO content of GFZ2 is more than GFZ1. Actually, the increase of zinc oxide nanoparticles increases the electron excitation rate and also increases the number of electron–hole pairs. The same results can be obtained for the other experimental pH (pH = 7 and pH = 11) and photocatalysts weight fraction (0.2%wt and 0.3%wt).
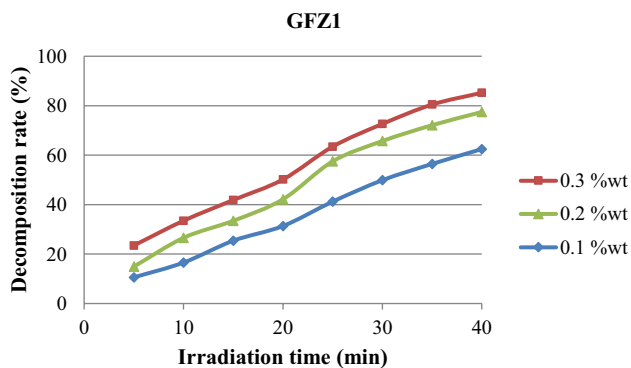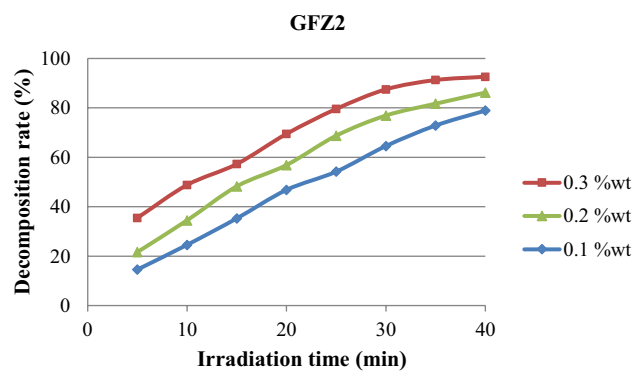

Fig. 11 The variation of MO decomposition rate with respect to the irradiation time and weight fraction of GFZ2

Response surface study

The surface response method (RSM) is one of the most common methods of statistical analysis, which is used to investigate the changes in the response to the simultaneous changes of two of the effective factors. In this case, the third factor remains at a constant level. Figures 13 and 14 depict the response surface of the MO decomposition rate using GFZ1 and GFZ2, respectively. Figures 13a and 14a show the effect of simultaneous changes in time and weight fraction of the GFZ1 and GFZ2, respectively. Based on these Figures, it can be deducted that increasing the irradiation time and the weight fraction of both the GFZ1 and GFZ2 as photocatalysts leads to an increase in the decomposition rate of MO. The increase in the decomposition rate can be attributed to the increase in the amount of generated electron holes and active radical species (Abbasi 2021a, 2022b). The changes in the decomposition rate of methyl orange with respect to time and pH using the GFZ1 and GFZ2 can be seen in Figs. 13b and 14b, respectively. It is clear that the changes in MO decomposition rate using both types of
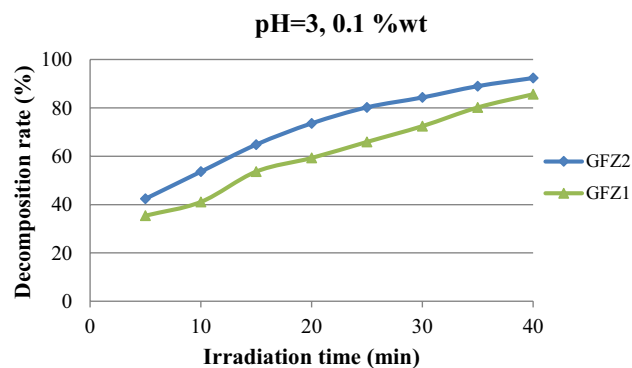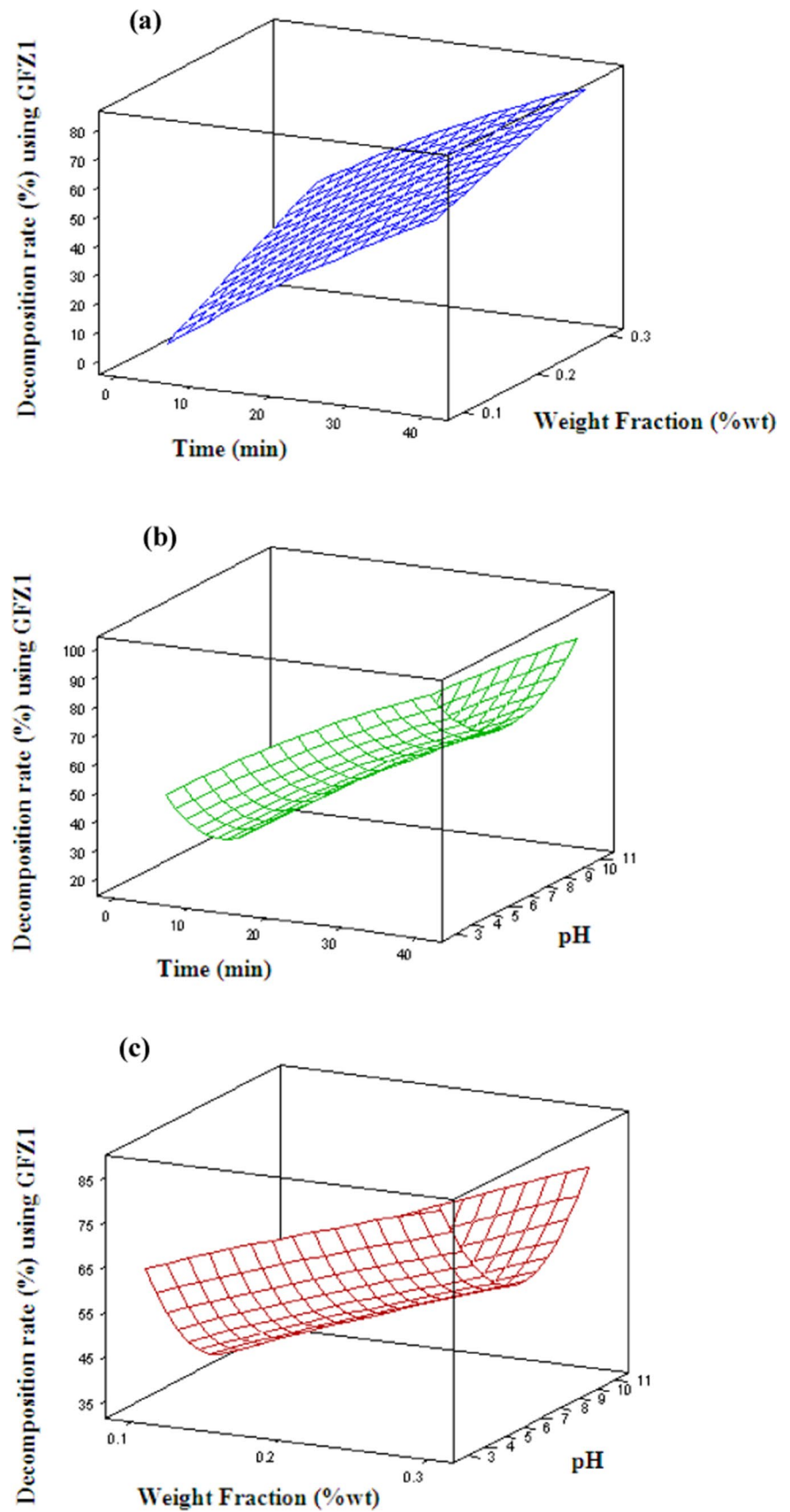

Fig. 10 The variation of MO decomposition rate with respect to the irradiation time and weight fraction of GFZ1

Fig. 12 The comparison between the changes MO degradation using GFZ1 and GFZ2, at pH = 3 and 0.1%wt

Fig. 13 Response surface of the MO decomposition rate using GFZ1 with respect to (**a**): time and weight fraction, (**b**): time and pH, (**c**): weight fraction and pH

Fig. 14 Response surface of the MO decomposition rate using GFZ2 with respect to (**a**): time and weight fraction, (**b**): time and pH, (**c**): weight fraction and pH
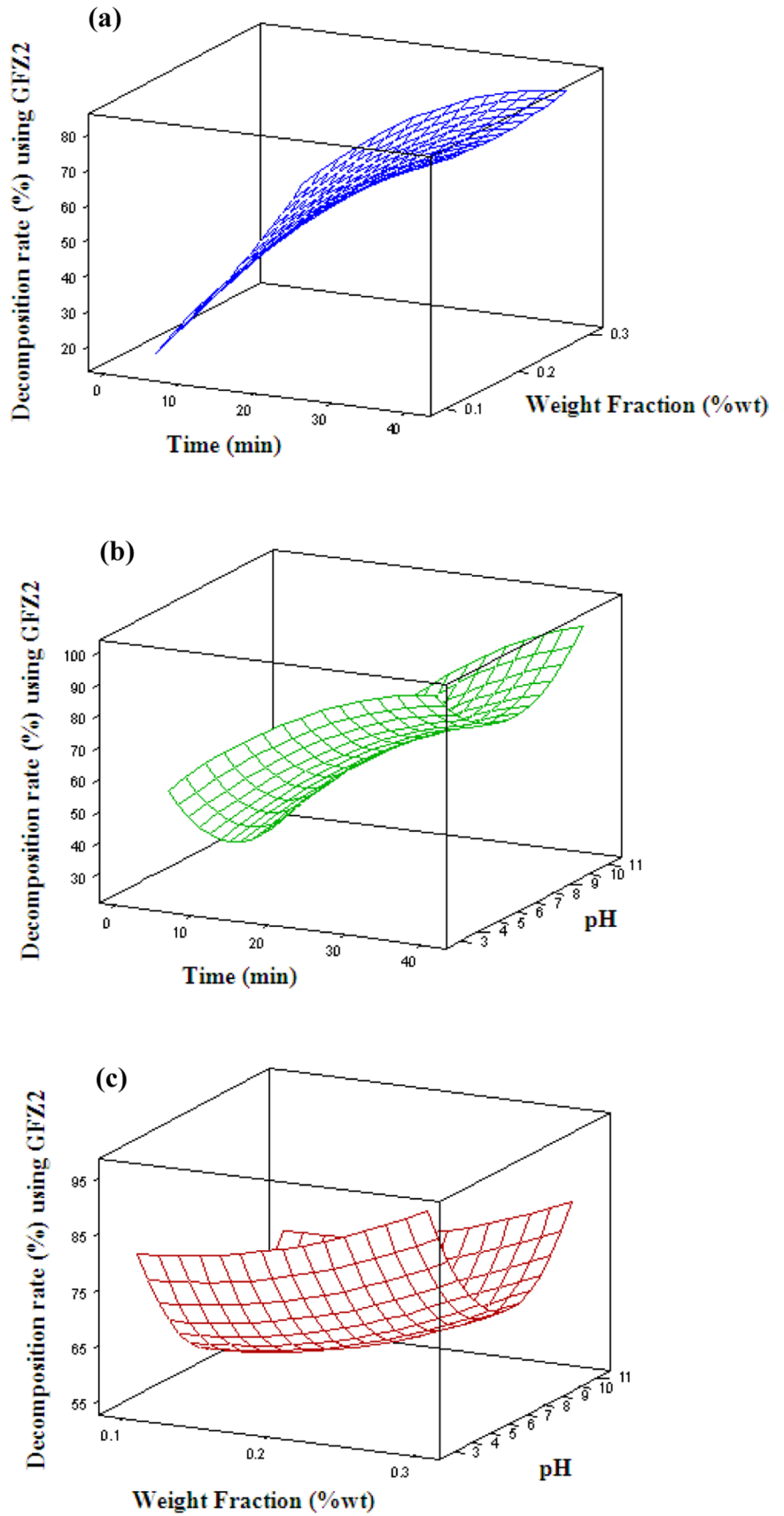
photocatalysts are significantly influenced by the pH of the suspension. The order of increase in decomposition rate in different pH is $pH = 3 > pH = 11 > pH = 7$. According to the obtained results, it can be concluded that the amount of MO removal in neutral conditions is at the lowest possible level. This is due to the reduction of surface charge and free hydrogen ions in neutral conditions. In fact, by reducing the surface charge, the dispersibility of the photocatalyst in the suspension containing MO decreases, as a result, the effective contact of MO with the surface of the photocatalyst decreases (Abbasi 2020; Abbasi et al. 2017b). Therefore, the degradation efficiency of MO in neutral conditions decreased significantly. The effect of increasing the photocatalyst weight fraction and pH on the MO decomposition rate in the presence of the GFZ1 and GFZ2 is presented in Figs. 13c and 14c, respectively. Increasing the weight fraction of both photocatalysts in the suspension containing MO has a direct effect on increasing the active contact surface to connect the pollutant to the photocatalyst. Also, the surface that is exposed to the radiation of the light source to excite the electrons can be increased. Therefore, both of the mentioned factors increase the decomposition rate of MO with increasing photocatalyst concentration.

Conclusions

Semiconductor nanoparticles play an important role in the decomposition of dye pollutants in aqueous solutions. The basis of semiconductors is to excite the electrons of the valence layer with light that has a higher energy than the band gap of semiconductor in order to decompose the dye organic pollutants. Therefore, the stability of the created electron–hole pairs is effective in improving the performance of the photocatalyst. In this research, we synthesize magnetic photocatalysts on the surface of graphene oxide. This action increases the separation of produced electrical charges and increases the decomposition efficiency of methyl orange as a model pollutant. Also, in order to study the effect of photocatalytic ZnO nanoparticles on the structure of the synthesized magnetic photocatalyst, two types of samples (GFZ1 and GFZ2) are synthesized, and the content of ZnO nanoparticles in GFZ2 is more than that of GFZ1. Examining the parameters affecting the decomposition rate, including irradiation time and photocatalyst weight fraction, shows that the decomposition rate of MO is directly affected by changes in irradiation time and weight fraction. While there is no uniform trend between pH changes and decomposition rate. As the pH increases from the acidic range ($pH = 3$) to the neutral condition ($pH = 7$), the rate of pollutant decomposition decreases, and then with the increase of pH to the alkaline range ($pH = 11$), an increasing trend is observed. Also, the results showed that the decomposition rate of

methyl orange has a direct relationship with the amount of ZnO nanoparticles in the sample. Therefore, GFZ2 has more photocatalytic activity compared to GFZ1.

Data availability The authors confirm that the data supporting the findings of this study are available within the article.

Declarations

Conflict of interest We pledge that none of the authors of this article have any financial or personal relationship with anyone or an institution that would lead to a negative impact on this study.

References

Abareshi M et al (2010) Fabrication, characterizationandmeasurementof thermal conductivity of Fe_3O4 nanofluids. J Magn Magn Mater 322:3895–3901

Abbasi S (2018) Investigation of the enhancement and optimization of the photocatalytic activity of modified TiO_2 nanoparticles with SnO_2 nanoparticles using statistical method. Mater Res Express 5:066302

Abbasi S (2019) Photocatalytic activity study of coated Anatase-Rutile Titania nanoparticles with nanocrystalline tin dioxide based on the statistical analysis. Environ Monit Assess 191(4):206–218

Abbasi S (2020) Adsorption of dye organic pollutant using magnetic ZnO embedded on the surface of graphene oxide. J Inorg Organomet Polym Mater 30:1924–1934

Abbasi S (2021a) Response surface methodology for photo degradation of methyl orange using magnetic nanocomposites containing zinc oxide. J Cluster Sci 32:805–812

Abbasi S (2021b) Improvement of photocatalytic decomposition of methyl orange by modified MWCNTs, prediction of degradation rate using statistical models. J Mater Sci Mater Electron 32:14137–14148

Abbasi S (2022a) The degradation rate study of methyl orange using MWCNTs@TiO_2 as photocatalyst, application of statistical analysis based on Fisher's F distribution. J Cluster Sci 33:593–602

Abbasi S, Hasanpour M (2017a) The effect of pH on the photocatalytic degradation of methyl orange using decorated ZnO

nanoparticles with SnO_2 nanoparticles. J Mater Sci Mater Electron 28(2):1307–1314

Abbasi S, Hasanpour M (2017b) Variation of the photocatalytic performance of decorated MWCNTs (MWCNTs-ZnO) with pH for photo degradation of methyl orange. J Mater Sci: Mater Electron 28(16):11846–11855

Abbasi S et al (2015) Synthesis of TiO_2 nanoparticles and decorated multiwalled carbon nanotubes with various content of rutile titania. Synth React Inorg, Met-Org, Nano-Met Chem 45:1539–1548

Abbasi S, Ekrami-Kakhki M-S, Tahari M (2017) Modeling and predicting the photodecomposition of methylene blue via $ZnO–SnO_2$ hybrids using design of experiments (DOE). J Mater Sci: Mater Electron 28(20):15306–15312

Abbasi S, Hasanpour M, Kakhki MSE (2017b) Removal efficiency optimization of organic pollutant (methylene blue) with modified multi-walled carbon nanotubes using design of experiments (DOE). J Mater Sci: Mater Electron 28(13):9900–9910

Abbasi S, Ekrami-Kakhki M-S, Tahari M (2019) The influence of ZnO nanoparticles amount on the optimisation of photo degradation of methyl orange using decorated MWCNTs. Progress Ind Ecol Int J 13(1):3–15

Abbasi S et al (2020) Synthesis of magnetic Fe_3O_4@ZnO@graphene oxide nanocomposite for photodegradation of organic dye pollutant. Int J Environ Anal Chem 100(2):225–240

Abbasi S et al (2021) Application of the statistical analysis methodology for photodegradation of methyl orange using a new nanocomposite containing modified TiO2 semiconductor with SnO_2. Int J Environ Anal Chem 101(2):208–224

Abbasi S et al. (2022b) Evaluation of the dependence of methyl orange organic pollutant removal rate on the amount of titanium dioxide nanoparticles in MWCNTs-TiO$_2$ photocatalyst using statistical methods and Duncan's multiple range test. Int J Environ Anal Chem

Abdel-Messih MF, Ahmed MA, El-Sayed AS (2013) Photocatalytic decolorization of Rhodamine B dye using novel mesoporous $SnO_2–TiO_2$ nano mixed oxides prepared by sol–gel method. J Photochem Photobiol A Chem 260:1–8

Dastan D, Panahi SL, Chaure NB (2016) Characterization of titania thin films grown by dip-coating technique. J Mater Sci: Mater Electron 27:12291–12296

Dastan D, Chaure N, Kartha M (2017) Surfactants assisted solvothermal derived titania nanoparticles: synthesis and simulation. J Mater Sci: Mater Electron 28:7784–7796

Fakhrzad M et al (2019) Synthesis of Zn_2SnO_4 nanoparticles used for photocatalytic purposes. Mater Res Express 6:095037

Gan L et al (2018) Graphene oxide incorporated alginate hydrogel beads for the removal of various organic dyes and bisphenol A in water. Colloid Polym Sci 296:607–615

Gao P, Sun DD (2014) Hierarchical sulfonated graphene oxide–TiO_2 composites forhighly efficient hydrogen production with a wide pH range. Appl Catal B-Environ 147:888–896

Ghaderi A, Abbasi S, Farahbod F (2015) Synthesis of SnO_2 and ZnO nanoparticles and SnO_2-ZnO hybrid for the photocatalytic oxidation of methyl orange. Iran J Chem Eng 12(3):96–105

Ghaderi A, Abbasi S, Farahbod F (2018) Synthesis, characterization and photocatalytic performance of modified ZnO nanoparticles with SnO_2 nanoparticles. Mater Res Express 5:065908

Kim SP, Choi MY, Choi HC (2015) Characterization and photocatalytic performance of SnO_2-CNTnanocomposites. Appl Surf Sci 357:302–308

Navidpour AH et al (2019) Novel photocatalytic coatings based on tin oxide semiconductor. Surf Eng 35(3):216–226

Reddy DA, Ma R, Kim TK (2015) Efficient photocatalytic degradation of methylene blue by heterostructured $ZnO–RGO/RuO_2$ nanocomposite under the simulated sunlight irradiation. Ceram Int 41:6999–7009

Roozban N, Abbasi S, Ghazizadeh M (2017a) Statistical analysis of the photocatalytic activity of decorated Multi-Walled carbon nanotubes with ZnO nanoparticles. J Mater Sci Mater Electron 28(8):6047–6055

Roozban N, Abbasi S, Ghazizadeh M (2017b) The experimental and statistical investigation of the photo degradation of methyl orange using modified MWCNTs with different amount of ZnO nanoparticles. J Mater Sci Mater Electron 28(10):7343–7352

Tao L et al (2023) Metal-decorated InN monolayer senses N_2 against CO_2. ACS Appl Mater Interfaces 15:12534–12544

Wang X, Yao S, Li X (2009) Sol-gel Preparation of CNT/ZnO nanocomposite and its photocatalytic property. Chin J Chem 27:1317–1320

Yuan NY et al (2012) High conductive ethylene vinyl acetate composites filled with reduced graphene oxide and polyaniline. Compos Part A 43:2183–2188

Zak AK et al (2011) Synthesis and characterization of ZnO nanoparticles prepared in gelatin media. Mater Lett 65:70–73

Zhu G et al (2015) A facile synthesis of ZnO/CNTs hierarchical mircosphere composites with enhanced photocatalytic degradation of methylene blue. RSC Adv 5(89):72476–72481